International Journal of Theoretical and Applied Mathematics
2026, Vol. 12, No. 2, pp. 37–45
https://doi.org/10.11648/j.ijtam.20261202.11

SciencePG
Science Publishing Group

Research Article

Local Thermal Nonequilibrium and Anisotropy Effects on Convective Instability of Maxwell Fluid

Nagappa Enagi[1, *], Sridhar Kulkarni[2]

[1]Department of Mathematics, KRCE Society's Arts and Science College, Bailhongal, India
[2]Department of Mathematics, Government First Grade College, Paschapur, India

Abstract

Thermal convection in fluid-saturated porous media has attracted considerable attention due to its wide-ranging applications in engineering and geophysical systems, such as geothermal energy extraction, underground contaminant transport, nuclear waste disposal, and heat exchangers. In these systems, buoyancy-driven flow arises when a temperature gradient is imposed across the medium. The onset of convection is primarily governed by the Rayleigh number, which quantifies the balance between thermal driving forces and dissipative effects, including viscosity and thermal diffusion. Conventional studies often assume local thermal equilibrium (LTE) between the solid matrix and the saturating fluid. However, this assumption becomes inadequate in many practical situations where the heat exchange between the two phases is not instantaneous. To overcome this limitation, the concept of local thermal non-equilibrium (LTNE) has been introduced, wherein separate energy equations are employed for the solid and fluid phases, allowing a more realistic representation of interphase heat transfer. Moreover, porous media encountered in practical applications are frequently anisotropic, with permeability and thermal conductivity varying with direction. Such anisotropy significantly influences both fluid flow and heat transport characteristics. The complexity of the problem is further enhanced when non-Newtonian fluids, particularly Maxwell fluids, are considered. Due to their viscoelastic nature, these fluids introduce additional parameters, such as stress relaxation time, which play a crucial role in determining the stability behavior of the system. Therefore, a comprehensive analysis that simultaneously incorporates LTNE effects, anisotropy, and non-Newtonian fluid behavior is essential for accurately predicting the onset of convection and gaining deeper insight into the associated stability mechanisms in porous media systems.

Keywords

Convection, Anisotropy, Maxwell Fluid, Thermal Non-equilibrium

1. Introduction

Thermal convection in porous media is of significant interest due to its applications in geothermal systems, petroleum reservoirs, and thermal engineering processes. The classical Darcy framework has been extended to incorporate realistic effects such as anisotropy, rotation, local thermal non-equilibrium (LTNE), and non-Newtonian fluid behavior.

Kulkarni (2013) [1] first analyzed unsteady convection in a

*Correspondence: Nagappa Enagi (nkenagi@gmail.com)

Received: 3 April 2026; **Accepted:** 20 April 2026; **Published:** 16 May 2026

rotating anisotropic porous layer using an LTNE model, followed by Shivakumara et al. (2015) [2], who demonstrated the importance of inter-phase heat transfer in such systems. The role of inclination and internal heat generation in anisotropic media was later examined by Storesletten and Rees (2019) [4]. Around the same period, Chavaraddi et al. (2019) [3] studied couple stress fluid effects under LTNE conditions.

Subsequent studies focused on non-Newtonian fluids and thermal effects. Shivakumara and Sureshkumar (2020) [5] and Kumar and Singh (2020) [6] investigated Maxwell and viscoelastic fluids, while Shehzad et al. (2021) [7] analyzed anisotropic permeability effects. In 2022, significant contributions were made by Shivakumara et al. [8], Enagi et al. [9], Chen and Pan [10], Zhang and Li [11], Chavaraddi et al. [12], and Ravish et al. [13], emphasizing LTNE, internal heating, and fluid elasticity.

Recent works include Enagi et al. (2023) [14], Enagi et al. (2024) [15], Kumar and Gupta (2024) [16], and Kousalya and Saravanan (2024) [17], addressing advanced fluid models and anisotropic effects. Further developments in magneto-convection and rotating systems were reported by Bixaathi and Babu (2025) [18] and Enagi and Kulkarni (2025) [19].

Despite these extensive studies, the combined effects of anisotropy, rotation, LTNE conditions, and complex non-Newtonian fluid behavior are not yet fully understood. Therefore, the present study aims to investigate the onset of thermal convection in an anisotropic porous medium under LTNE conditions, taking into account the relevant physical parameters governing system stability. The results are expected to provide a better understanding of convective mechanisms and contribute to the design and optimization of systems involving porous media.

2. Governing Equations

A porous layer contained in two horizontal free surfaces of distance ‘h’. A Maxwell fluid is studied under the influence of anisotropy with vertically downward gravity force ‘g’ acting on it. The lower surface temperature $\mathcal{T}_\ell$ is heated from below, the upper surface temperature $\mathcal{T}_u$ is allow to cool from top ($\mathcal{T}_\ell > \mathcal{T}_u$). We assume that the solid and fluid medium are not in LTE. We use a two-field modeled equation for temperature. Thus, the corresponding basic governing equations become.

$$\nabla \cdot V = 0 \tag{1}$$

$$\left(1+\lambda\frac{\partial}{\partial t}\right)\left(\frac{\rho_0}{\varepsilon}\frac{\partial V}{\partial t}+\nabla p-\rho g\right)+\frac{\mu_f}{\mathcal{K}}V-\mu_e\nabla^2 V=0 \tag{2}$$

$$\varepsilon(\rho_c)_f\frac{\partial \mathcal{T}_f}{\partial t}+(\rho_c)_f(V\cdot\nabla)\mathcal{T}_f=\varepsilon k_{fh}\nabla^2\mathcal{T}_f+n(\mathcal{T}_s-\mathcal{T}_f) \tag{3}$$

$$(1-\varepsilon)(\rho_c)_s\frac{\partial \mathcal{T}_s}{\partial t}=(1-\varepsilon)k_{sh}\nabla^2\mathcal{T}_s-n(\mathcal{T}_s-\mathcal{T}_f) \tag{4}$$

$$\rho_f=\rho_0\left[1-\beta_1\left(\mathcal{T}_f-\mathcal{T}_u\right)\right] \tag{5}$$

The pressure term in (2) will be eliminating by operating curl twice on (2)also equations (3) to (5) make non dimensional by using the following transformations and render the resulting equations.

$$(x,y,z)=h(x^*,y^*,z^*),(u,v,w)=\frac{\varepsilon \mathrm{k}_f}{h(\rho_o c)_f}(u^*,v^*,w^*),$$

$$p=\frac{\mathrm{k}_f\mu}{(\rho_o c)_f K}p^*\ \mathcal{T}_f=(\mathcal{T}_\ell-\mathcal{T}_u)\ \mathcal{T}_f^*+\mathcal{T}_u,$$

$$\mathcal{T}_s=(\mathcal{T}_\ell-\mathcal{T}_u)\mathcal{T}_s^*+\mathcal{T}_u,\mathrm{t}=\frac{(\rho_o c)_f h^2}{\mathrm{k}_f}t^* \tag{6}$$

Using (6) we get below dimensionless equations from (1)-(5).

$$\left(1+\lambda\frac{\partial}{\partial t}\right)\left(\frac{1}{P_{rD}}\frac{\partial}{\partial t}(\nabla^2 w)-R_a\nabla_1^2\mathcal{T}_f\right)+\nabla_1^2 w+\frac{1}{\varepsilon}\frac{\partial^2 w}{\partial z^2}=0 \tag{7}$$

$$\frac{\partial \mathcal{T}_f}{\partial t}+(\nabla\cdot V)\mathcal{T}_f=\eta_f\nabla_1^2\mathcal{T}_f+\frac{\partial^2\mathcal{T}_f}{\partial z^2}+H\left(\mathcal{T}_s-\mathcal{T}_f\right) \tag{8}$$

$$\alpha\frac{\partial \mathcal{T}_s}{\partial t}+\eta_s\nabla^2\mathcal{T}_s+\frac{\partial^2 k}{\partial z^2}-\gamma H\left(\mathcal{T}_s-\mathcal{T}_f\right)=0 \tag{9}$$

$$R_L=\frac{\rho\beta g(\mathcal{T}_l-\mathcal{T}_u)h\mathcal{K}}{\varepsilon\mu_f \mathrm{k}_f},\Gamma=\frac{\lambda \mathrm{k}_f}{(\rho_c)_f h^2},\gamma=\frac{\varepsilon \mathrm{k}_f}{(1-\varepsilon)\mathrm{k}_s},\ \eta_f=\frac{\mathrm{k}_{fx}}{\mathrm{k}_{fz}},\ \eta_s=\frac{\mathrm{k}_{sx}}{\mathrm{k}_{sz}},\xi=\frac{\mathcal{K}_x}{\mathcal{K}_z} \tag{10}$$

For simplification purpose we remove stars from the above equations.

2.1. Properties of Basic State

The equations given below are the assumptions of inactive basic state.

$$u=v=w=0,\mathcal{T}_f=\mathcal{T}_{fb}(z),\mathcal{T}_s=\mathcal{T}_{sb}(z) \tag{11}$$

The fluid and solid medium basic state temperatures are $\mathcal{T}_{fb}$ *and* $\mathcal{T}_{sb}$ respectively satisfy the following equations.

$$\frac{d^2\mathcal{T}_{fb}}{dz^2}+N\left(\mathcal{T}_{sb}-\mathcal{T}_{fb}\right)=0 \tag{12}$$

$$\frac{d^2\mathcal{T}_{fb}}{dz^2}+\gamma N(\mathcal{T}_{sb}-\mathcal{T}_{fb})=0 \tag{13}$$

with the boundary conditions are

$$\mathcal{T}_{fb}=\mathcal{T}_{sb}(z)=1\ at\ z=0,\mathcal{T}_{fb}=\mathcal{T}_{sb}(z)=0\ at\ z=1 \tag{14}$$

The basic state solutions satisfying the conditions (14) are

$$\mathcal{T}_{fb} = \mathcal{T}_{sb}(z) = (1 - z) \quad (15)$$

2.2. Perturbation Solution

The basic state having some small disturbance and therefore the temperature and velocity components under this state are given by

$$(u, v, w) = (\grave{u}, \grave{v}, \grave{w}), \mathcal{T}_f = \mathcal{T}_{fb} + \theta, \mathcal{T}_s = \mathcal{T}_{sb} + \phi \quad (16)$$

Where the ` denote the perturbations quantity. Substituting equation (16) into(7) to (9) and using the result of basic state, we get.

$$\left(1 + \Gamma\frac{\partial}{\partial t}\right)\left(\frac{1}{P_{rD}}\frac{\partial}{\partial t}(\nabla^2 w) - R_L\nabla_1^2\theta\right) + \nabla_1^2 w + \frac{1}{\xi}\frac{\partial^2 w}{\partial z^2} = 0 \quad (17)$$

$$\frac{\partial\theta}{\partial t} - \eta_f\nabla_1^2\theta - \frac{\partial^2\theta}{\partial z^2} - N(\Phi - \theta) - w = 0 \quad (18)$$

$$\alpha\frac{\partial\Phi}{\partial t} + \eta_s\nabla_1{}^2\Phi + \frac{\partial^2\Phi}{\partial z^2} - \gamma N(\Phi - \theta) = 0 \quad (19)$$

Now Evaluating equations (17) to (19) for isothermal boundaries. Thus, the endconditions are

$$\left.\begin{array}{l} w = 0 \; at \; z_1 = 0, 1 \\ \theta = \Phi = 0 \; at \; z_1 = 0, 1 \end{array}\right\} \quad (20)$$

2.3. Linear Stability Analysis

It is assumed the normal mode expressions for the eigen values problems defined by equations {(17) - (19)} subject to the boundary conditions (20) are in the form

$$[w, \theta, \Phi] = [\mathcal{U}(z), \mathcal{V}(z), \mathcal{W}(z)]e^{i(lx+my)\sin\pi z + \omega t} \quad (21)$$

Where $a = \sqrt{l^2 + m^2}$ represents the wave numbers and ω is the growth rate, which is assumed to be real. Substituting equations (21) in equations (17) to (19) we get equations

$$(1 + \Gamma\omega)\left(\frac{\omega}{P_r}(D^2 - a^2)\mathcal{U} - R_a a^2\mathcal{V}\right) - (1 + \Lambda\Gamma\omega)a^2\mathcal{W} = 0 \quad (22)$$

$$(D^2 - a^2\eta_f - \omega)\mathcal{V} + \mathcal{W} + N(\mathcal{W} - \mathcal{V}) = 0 \quad (23)$$

$$(D^2 - a^2\eta_s - \alpha\omega)\mathcal{W} - \gamma N(\mathcal{W} - \mathcal{V}) = 0 \quad (24)$$

Where $D = \frac{d}{dz}$ now the boundary conditions become

$$\mathcal{U} = \mathcal{V} = \mathcal{W} = 0 \text{ for } z=0, 1 \quad (25)$$

The assumed solutions of, $\mathcal{U}$, $\mathcal{V}$, $\mathcal{W}$ are in the form

$$\begin{bmatrix}\mathcal{U}\\ \mathcal{V}\\ \mathcal{W}\end{bmatrix} = \begin{bmatrix}X\\ Y\\ Z\end{bmatrix} sin\pi z \text{ (n=1, 2, 3, 4…….)} \quad (26)$$

If n=1 and the boundary conditions (25) therefore substitute (26) in the equations (22) -(24) we get the following matrix.

$$\begin{bmatrix}\frac{\omega\delta^2\xi}{P_r} + \frac{C_1}{1+\Gamma\omega} & -R_L a^2\xi & 0\\ 1 & -(C_2 + \omega + N) & N\\ 0 & \gamma N & -(C_3 + \alpha\omega + \gamma N)\end{bmatrix}\begin{bmatrix}X\\ Y\\ Z\end{bmatrix} = \begin{bmatrix}0\\ 0\\ 0\end{bmatrix} \quad (27)$$

Where $\delta^2 = a^2 + \pi^2$, is the total wave number, $C_1 = \pi^2 + a^2\xi$, $C_2 = \pi^2 + a^2\eta_f, C_3 = \pi^2 + a^2\eta_s$.

For the non-trivial solution, we equating the coefficient of the above matrix equation (27) to zero, we get.

$$R_L = \frac{1}{\xi a^2}\left[\frac{\omega\delta^2\xi}{Pr} + \frac{C_1}{1+\Gamma\omega}\right]\left[C_2 + \omega + \frac{N(C_3+\alpha\omega)}{(C_3+\alpha\omega+\gamma N)}\right] \quad (28)$$

Setting $\omega = i\omega_i$ in equation (28) and from denominator the complex term can be removed we get

$$R_L = \Delta_1 + i\omega\Delta_2 \quad (29)$$

$$\Delta_1 = \frac{1}{a^2\xi}\begin{bmatrix}\frac{C_1}{1+\Gamma^2\omega^2}\left(C_2 + \Gamma\omega^2 + \frac{N(C_3{}^2 + C_3\gamma N + \alpha^2\omega^2)}{(C_3+\gamma N)^2 + \alpha^2\omega^2}\right)\\ -\frac{\delta^2\xi\omega^2}{P_r}\left(-\frac{\Gamma C_1}{1+\Gamma^2\omega^2}\right)\end{bmatrix}\left(1 + \frac{\alpha\gamma N^2}{(C_3+\gamma N)^2 + \alpha^2\omega^2}\right) \quad (30)$$

$$\Delta_2 = \frac{C_1}{a^2\xi}\frac{\delta^2\xi(1+\Gamma^2\omega^2) - \Gamma C_1 Pr}{Pr(1+\Gamma^2\omega^2)^2}\begin{bmatrix}\left(1 + \frac{\alpha\gamma N^2}{(C_3+\gamma N)^2 + \alpha^2\omega^2}\right)\\ \left(C_2 + \frac{N(C_3{}^2 + C_3\gamma N + \alpha^2\omega^2)}{(C_3+\gamma N)^2 + \alpha^2\omega^2}\right)\end{bmatrix} \quad (31)$$

Since R_L is a real number from (29) either $\omega_i = 0$ (Stationary convection) or $\Delta_2 = 0$ ($\omega_i \neq 0$, oscillatory convection).

a) For stationary mode of convection

For the stationary convection, $\omega_i = 0$ then equation (29) reduces to

$$R_{L,st} = \frac{C_1}{a^2\xi}\left(C_2 + \frac{C_3 N}{C_3+\gamma N}\right) \tag{32}$$

b) For oscillatory mode of convection

For oscillatory mode of convection $\Delta_2 = 0$ ($\omega_i \neq 0$) and hence this yields the dispersion relation of the form

$$b_1(\omega_i{}^2)^2 + b_2\omega_i{}^2 + b_3 = 0 \tag{33}$$

$$\text{and } \omega^2 = \frac{-b_2 \mp \sqrt{b_2{}^2 - 4b_1b_3}}{2b_1} \tag{34}$$

Where, $b1 = N\alpha^2\Gamma^2\delta^2\xi + \alpha^2\Gamma^2\delta^2\xi C_2$

$$b2 = N\alpha^2\delta^2\xi + Pr\alpha^2C_1 - NPr\alpha^2\Gamma C_1 + \alpha^2\delta^2\xi C_2 + N^2\gamma^2\Gamma^2\delta^2\xi C_2 - Pr\alpha^2\Gamma C_1C_2 + N\gamma^2\Gamma^2\delta^2\xi C_3 + N^2\gamma\Gamma^2\delta^2\xi + 2N\gamma\Gamma^2\delta^2\xi C_2C_3 + \Gamma^2a^2\delta^2\xi C_2C_3^2 + N\Gamma^2\delta^2\xi C_3\eta_s^2$$

$$b3 = N^2Pr\alpha\gamma C_1 + N^2Pr\gamma^2C_1 + N^2\gamma^2\delta^2\xi C_2 - N^2Pr\gamma^2\Gamma C_1C_2 + N\gamma^2\delta^2\xi C_3 + N^2\gamma\delta^2\xi C_3 + 2NPr\gamma C_1C_3 - NPr\gamma^2\Gamma C_1C_3 - N^2Pr\gamma\Gamma C_1C_3 + 2N\gamma\delta^2\xi C_2C_3 - 2NPr\gamma\Gamma C_1C_2C_3 + PrC_1C_3^2 + \delta^2\xi C_2C_3^2 - Pr\Gamma C_1C_2C_3^2 + a^2N\delta^2\xi C_3\eta_s^2 - a^2NPr\Gamma C_1C_3\eta_s^2 = 0$$

equation (29) becomes

$$R_{L,osc} = \frac{1}{a^2\xi}\left[\left(\frac{C_1}{1+\Gamma^2\omega^2}\right)\left(C_2 + \frac{N(C_3{}^2+C_3\gamma N+\alpha^2\omega^2)}{(C_3+\gamma N)^2+\alpha^2\omega^2}\right) - \omega^2\left(\frac{\delta^2\xi}{Pr} - \frac{\Gamma C_1}{1+\Gamma^2\omega^2}\right)\left(1 + \frac{\alpha\gamma N^2}{(C_3+\gamma N)^2+\alpha^2\omega^2}\right)\right] \tag{35}$$

3. Results and Discussion

The Rayleigh number expressions (32) and (35) analyses the behavior of several parameters and their effects on convection. Figures 1 to 5 show the marginal stability curves for distinct values of η_s, η_f, N, ξ & γ, with all other parameters held constant. The neutral curves are connected in a topological sense, and linear stability is determined by the critical Rayleigh number. If the Rayleigh number is less than its critical value, the system remains stable; otherwise, it becomes unstable.

Figures 1–3 illustrate the influence of η_s, η_f, & N on these marginal curves. It is observed that the minimum (critical) Rayleigh number increases as η_s, η_f, & N increase, indicating that thermal anisotropy in the solid and fluid phases and a higher interphase heat transfer coefficient N have a stabilizing effect on convection. Figures 4 and 5 show the effect of the mechanical anisotropy parameter ξ and the conductivity ratio γ. In these cases, the minimum Rayleigh number decreases as ξ and γ increase, indicating that mechanical anisotropy ξ and conductivity ratio γ have a destabilizing effect on the onset of convection.

Figures 6 and 7 show the effect of the heat transfer coefficient N on the critical Rayleigh number for different values of η_s, & η_f for both mode of convection. It is observed that, for larger values of η_s, & η_f the critical Rayleigh number increases for both mode of convection, indicating that thermal anisotropy in the solid and fluid phases stabilizes the system. Figure 8 shows the effect of N for different values of the diffusivity ratio α. The critical Rayleigh number increases as α increases for oscillatory convection, indicating that a larger diffusivity ratio α also enhances system stability.

Figures 9 - 11 show the impact of N on the critical Rayleigh number for the convection, for various values of conductivity ratio γ, stress relaxation time Γ and Prandtl number Pr for oscillatory convection. It is observed that decreasing γ, Γ and Pr leads to an increase in the critical Rayleigh number, meaning that the conductivity ratio γ, the stress relaxation time Γ and the Prandtl number Pr each have a destabilizing effect on the system.

Figures 12 - 17 demonstrate how the critical wave number a varies with N for distinct values of η_s, η_f, Γ, γ, α, and Pr. For very small or very large values of N, the critical wave number remains constant. At very small N, the solid phase stops affecting the thermal field of the fluid phase, effectively eliminating heat transfer between them. Conversely, at very large N, the solid and fluid phases are nearly at the same temperature, maximizing heat transfer between them. For intermediate values of N, the critical wave number reaches its maximum value. It is also noted that, as $N \to 0$ and $N \to \infty$, the critical wave number approaches the same limit only for γ, whereas for η_s, η_f, Γ, α, and Pr the low-N and high-N limits differ.

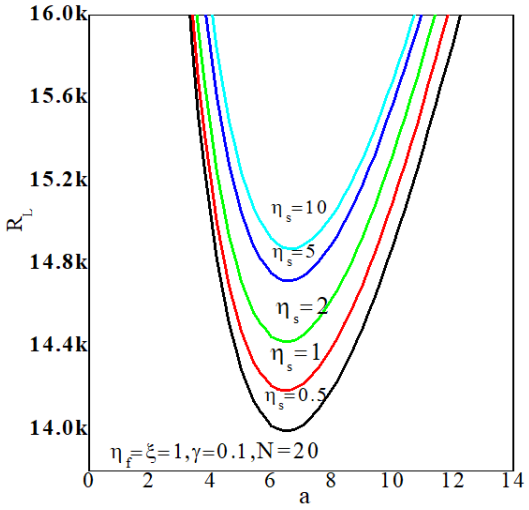

Figure 1. *Variation of R_L w.r.t 'a' for different values of η_s.*

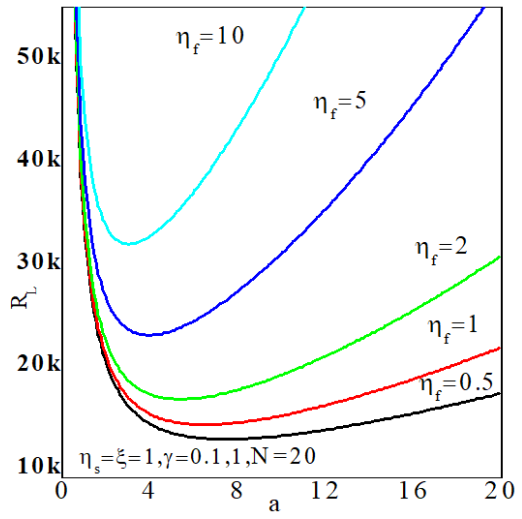

Figure 2. *Variation of R_L w.r.t 'a' for different values of η_f.*

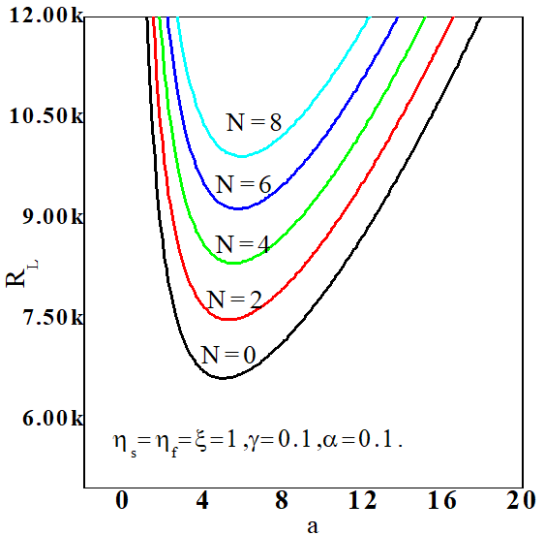

Figure 3. *Variation of R_L w.r.t 'a' for different values of N.*

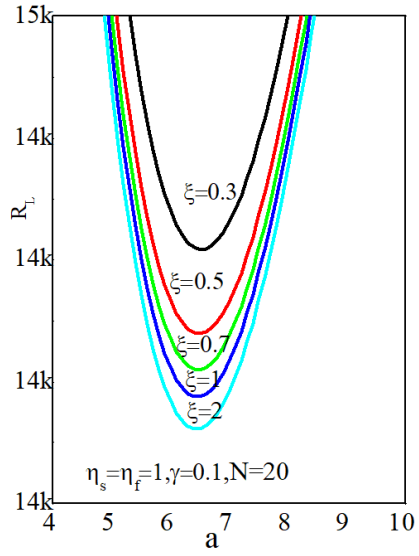

Figure 4. *Variation of R_L w.r.t 'a' for different values of ξ.*

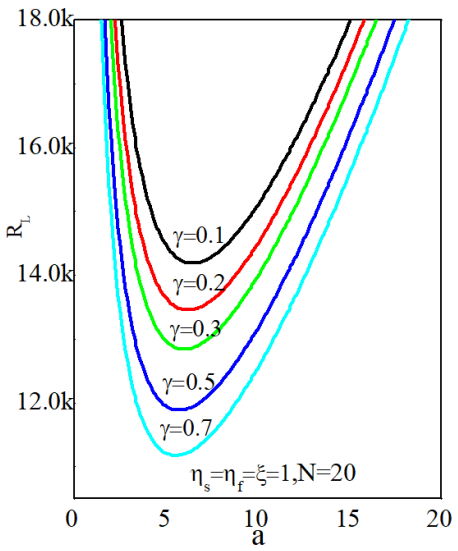

Figure 5. *Variation of R_L w.r.t 'a' for different values of γ.*

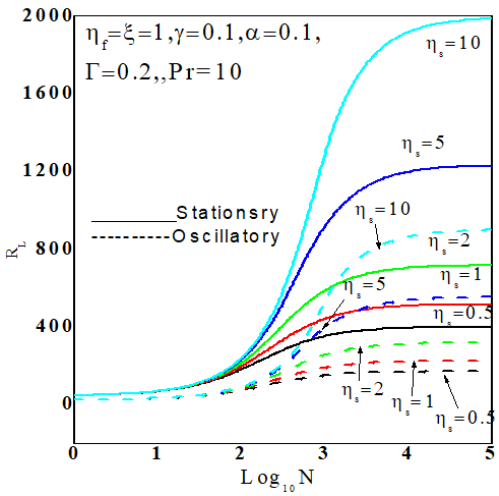

Figure 6. *Variation of RLos w.r.t N for different values of η_s.*

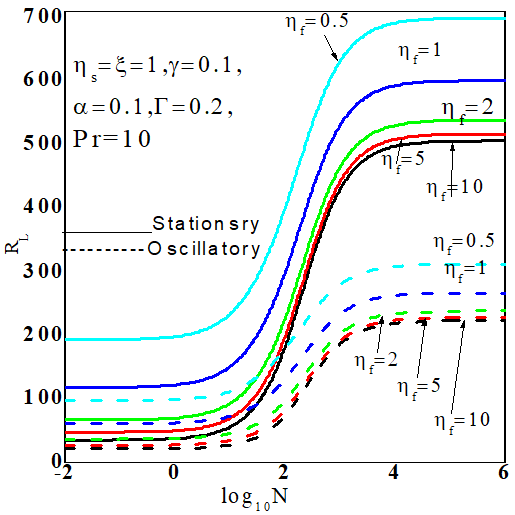

Figure 7. *Variation of RLos w.r.t N for different values of η_f.*

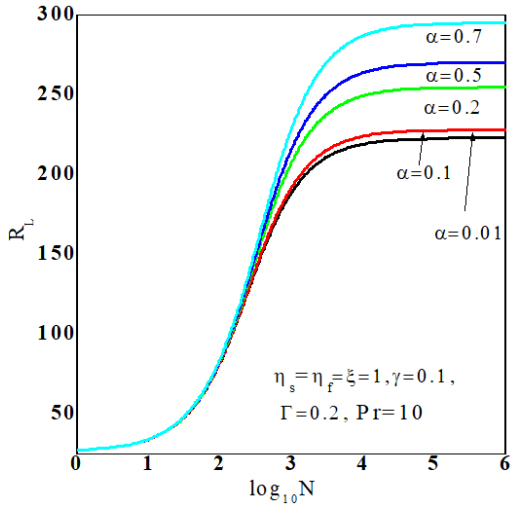

Figure 8. *Variation of RLos w.r.t N for different values of α.*

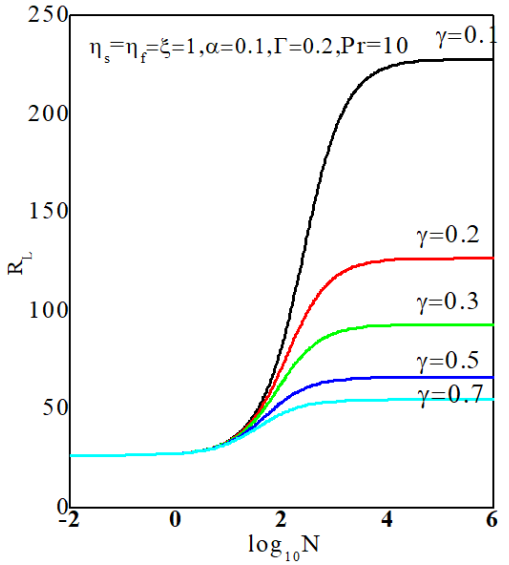

Figure 9. *Variation of RLos w.r.t N for different values of γ.*

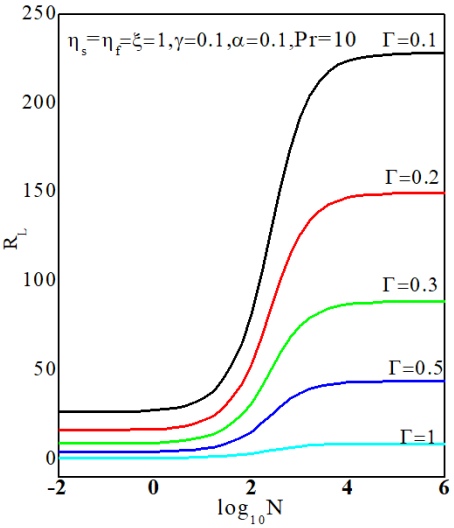

Figure 10. *Variation of RLos w.r.t N for different values of Γ.*

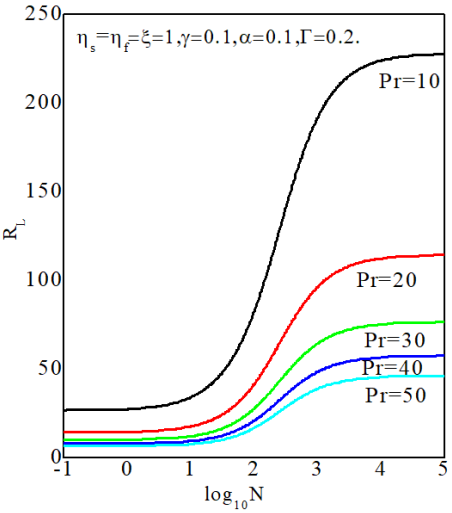

Figure 11. *Variation of RLos w.r.t N for different values of Pr.*

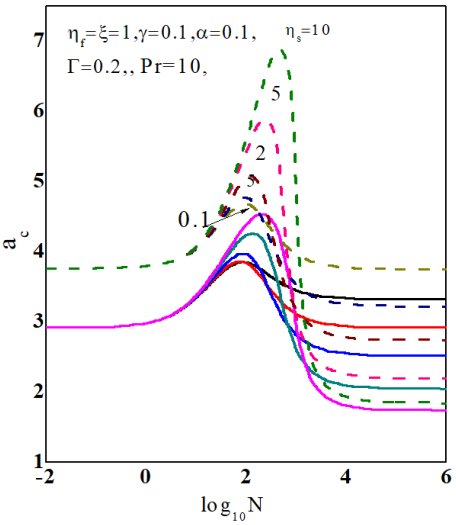

Figure 12. *Variation of 'ac' w.r.t N for different values of η_s.*

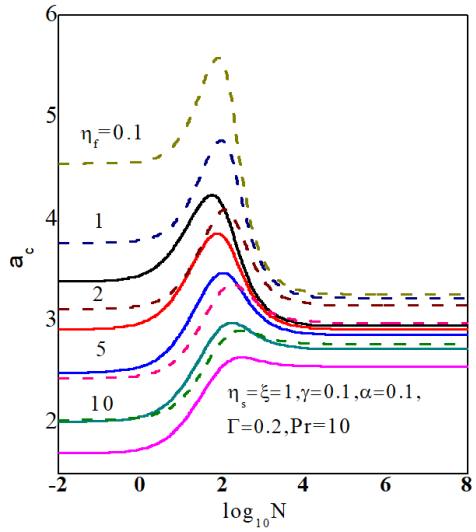

Figure 13. Variation of 'ac' w.r.t N for different values of η_f.

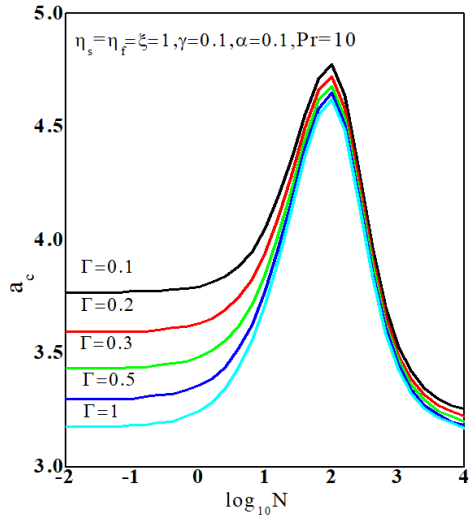

Figure 14. Variation of 'ac' w.r.t N for different values of Γ.

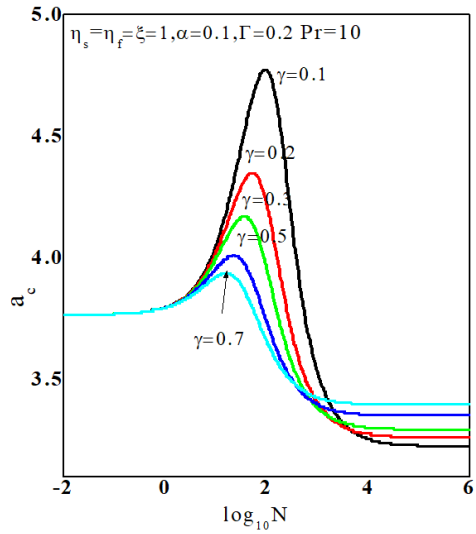

Figure 15. Variation of 'ac' w.r.t N for different values of γ.

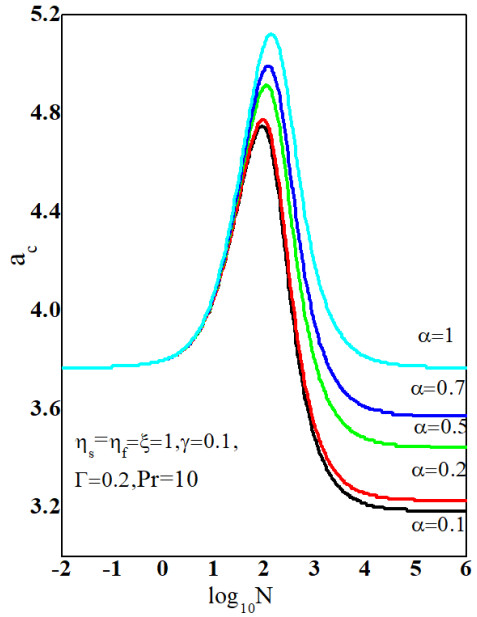

Figure 16. Variation of 'ac' w.r.t N for different values of α.

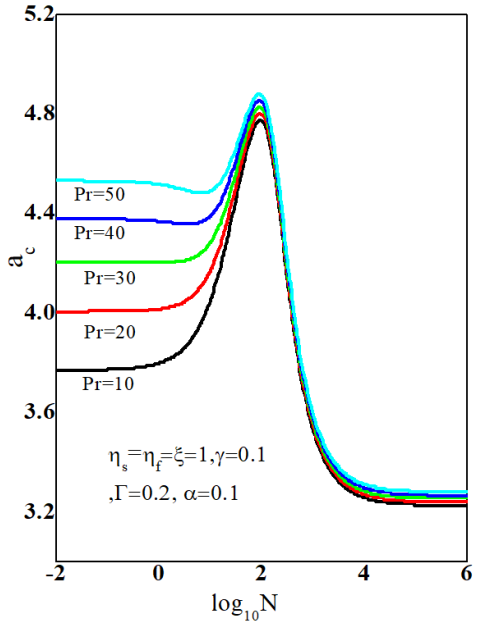

Figure 17. Variation of 'ac' w.r.t N for different values of Pr.

4. Conclusion

The thermal convection in an anisotropic Maxwellfluid contained in a porous layer is examined analytically. By applying the normal mode technique, the equations are linear. The study concludes that thermal anisotropy and diffusivity effects tend to stabilize the convective system, whereas mechanical anisotropy, conductivity ratio, and certain fluid properties can destabilize it. The interplay of these parameters governs the transition between stable and unstable convection, providing deeper insight into the control of convective processes in anisotropic porous media.

Abbreviations

a	Horizontal Wave Number, $\sqrt{l^2+m^2}$
c	Specific Heat
d	Height of the Porous Layer
g	Gravitational Acceleration
$\mathcal{K}$	Permeability Tensor, $\mathcal{K}h(ii+jj)+\mathcal{K}zkk$
k_f	Thermal Conductivity Tensor of Fluid Phase
k_s	Thermal Conductivity Tensor of Solid Phase
l,m	Wave Numbers in the x and y Direction Respectively
p	Pressure
V	Velocity Vector: (u, v, w)
$\mathcal{T}$	Temperature
t	Time
RL	Rayleigh Number, $\rho_0\beta d(\mathcal{T}_\ell-\mathcal{T}_u)\mathcal{K}/\varepsilon k_f\mu$
Ta	Taylor Number
P_r	Darcy-Prandtl Number,
H	Non-dimensional Inter Phase Heat Transfer Coefficient, $\frac{hd^2}{\varepsilon k_f}$
(x,y,z)	Space Coordinates
α	Diffusive Ratio
β	Coefficient of Thermal Expansion
γ	Porosity-modified Conductivity Ratio $\varepsilon k_f/(1-\varepsilon)\mathcal{K}$
ε	Porosity
μ	Fluid Viscosity
μ_c	Couple Stress Viscosity
μ_e	Effective Viscosity
υ	Kinematic Viscosity, μ/ρ_0
Γ	Non-dimensional Stress Relaxation Parameter $\lambda_1 k_f/(\rho_0 c)_f d^2=\lambda_1\kappa_f/d^2$
μ	Dynamic Viscosity
ν	Kinematic Viscosity, μ/ρ_0
κ	Thermal Diffusivity, $k_f/(\rho_0 c)_f$
ω	Frequency
ξ	Anisotropic Permeability Parameter, $\frac{\mathcal{K}_x}{\mathcal{K}_z}$
ω	Growth Rate
ψ	Stream function
φ	Non dime$nsional Temperature of Solid Phase
θ	Non dimen$sional Temperature of Fluid Phase
ρ	Fluid Density
l	Lower
s	Solid phase
c	Critical
b	Base state
h	Horizontal
f	Fluid phase
0	Reference
*	Dimensionless quantity
$\acute{u}$	Perturbed quantity
t	Time

Acknowledgments

The authors would like to thank principals and the management of our colleges for their valuable support and discussions. The authors declare that no specific funding was received for this work.

Author Contributions

Nagappa Enagi: Conceptualization, Methodology, Formal Analysis, Investigation, Visualization, Writing – original draft, Data curation, Software, Validation

Sridhar Kulkarni: Supervision, Project administration, Resources, Funding acquisition, Writing – review & editing

Conflicts of Interest

The authors declare that they have no known financial, commercial, or personal relationships that could have appeared to influence the work reported in this paper.

References

[1] Kulkarni Sridhar, (2013): Unsteady thermal convection in a rotating anisotropic porous layer using a thermal non equilibrium model. International Journal of Physics and Mathematical Science, 2277-211. https://doi.org/10.1007/s11242-004-5130-z

[2] I. S. Shivakumara, Lee Jinho, A. L. Mamatha and M. Ravish, Local thermal non equilibrium effects on thermal convection in rotating anisotropic porous layer, Appl. Mathematic and Computation 259 (2015), 838-857. https://doi.org/10.1016/j.amc.2015.03.023

[3] Krishna B. Chavaraddi, N. K. Enagi and Sridhar Kulkarni, On the onset of convection in a couple stress fluid saturated rotating anisotropic porous layer using thermal non equilibrium model, JP Journal of Heat and Mass Transfer 16(1) (2019), 125-142. http://dx.doi.org/10.17654/HM016010125

[4] Leiv Storesletten and D. A. S. Rees, Onset of convection in an inclined anisotropic porous layer with internal heat generation, Fluids 4(2) (2019), 75. https://doi.org/10.3390/fluids4020075

[5] Shivakumara, I. S., & Sureshkumar, S. (2020). Convective instability in a Maxwell fluid-saturated porous layer with internal heat generation. Journal of Non-Newtonian Fluid Mechanics, 281, 104292, https://doi.org/10.1016/j.jnnfm.2020.104292

[6] Kumar, J., & Singh, A. K. (2020). Double-diffusive convection in a viscoelastic fluid-saturated porous medium under LTNE conditions. International Journal of Heat and Mass Transfer, 152, 119512; https://doi.org/10.1016/j.ijheatmasstransfer.2020.119512

[7] Shehzad, S. A., Abbasi, F. M., & Hayat, T. (2021). Thermal instability of Maxwell fluid in porous media with anisotropic permeability. Physics of Fluids, 33(3), 033106. https://doi.org/10.1063/5.0042787

[8] Shivakumara, I. S., Ravish, M., & Lee, J. (2022). Combined effects of LTNE and anisotropy on convection in porous media. Transport in Porous Media, 141(1), 123–145. https://doi.org/10.1007/s11242-021-01665-2

[9] Enagi, N. K., Chavaraddi, K. B., Kulkarni, S. Effect of maximum density and internal heating on the stability of rotating fluid saturated porous layer using LTNE model. Heliyon. 2022; e09620. https://doi.org/10.1016/j.heliyon.2022.e09620

[10] Chen Yin, Panpan pan (2022): Thermal Convection for an Oldroyd-B Fluid in an Anisotropic Porous Medium Underlying a Fluid Layer, *J. Heat Transfer*, 144(11), 113601 https://doi.org/10.1115/1.4055242

[11] Zhang, Y., & Li, D. Thermal convection in anisotropic porous media with internal heat source. Applied Mathematics and Computation, 2022 419, 126865. https://doi.org/10.1016/j.amc.2021.126865

[12] K. B. Chavaraddi, N. K. Enagi and Sridhar Kulkarni, Non-equilibrium thermal convection in an anisotropic porous layer saturated with a viscoelastic fluid, AIP Conference Proceedings 2022. https://doi.org/10.1063/5.0095544

[13] N. K. Enagi, Krishna B. Chavaraddi, Sridhar Kulkarni, Couple stress fluid saturated rotating porous layer with internal heat generation and density maximum, JP Journal of Heat and Mass Transfer 35(1) (2023), 1-19. http://dx.doi.org/10.17654/0973576323039

[14] N. K. Enagi, Krishna B. Chavaraddi and Sridhar Kulkarni, The effect of anisotropy on Darcy-Brinkman convection in a Maxwell fluid saturated porous layer, Advances and Applications in Fluid Mechanics 31(1) (2024), 1-22. https://doi.org/10.17654/0973468624001

[15] Kumar, V., & Gupta, U: Stability analysis of viscoelastic fluid convection in anisotropic porous media under LTNE conditions. Journal of Thermal Analysis and Calorimetry, 2024, 149(2), 987–1002. https://doi.org/10.1007/s10973-023-12567-8

[16] M. Kousalya and S. Saravanan, Effect of gravity and anisotropy on the convective instability in nanofluid porous medium, Numerical Heat Transfer (2024). https://doi.org/10.1080/10407782.2024.2365424

[17] S. Bixaathi and A. B. Babu, Casson fluid flow of rotating magneto-convection in a vertical porous medium, Phys. Fluids 37(1) (2025), 014125. https://doi.org/10.1063/5.0231663

[18] N. K. Enagi and Sridhar Kulkarni, The effect of anisotropy on the stability of rotating fluid saturated porous layer using LTNE model, Advances and Applications in Fluid Mechanics 32(1) (2025), 19-35. https://doi.org/10.17654/0973468625002

[19] Ravish, M., Shivakumara, I. S., & Lee, J. Combined effects of LTNE and anisotropy on convection in porous media. Transport in Porous Media, 2022, 141(1), 123–145. https://doi.org/10.1007/s11242-021-01658-0